Fabrication of Multifunctional SiO$_2$@GN-Serum Composites for Chemo-Photothermal Synergistic Therapy

Yuwei Liu,[†,‡] Jing Bai,[†] Xiaodan Jia,[†] Xiue Jiang,*[,†] and Zhuo Guo*[,‡]

[†]State Key Lab of Electroanalytical Chemistry, Changchun Institute of Applied Chemistry, Chinese Academy of Sciences, Changchun, 130022, Jilin China

[‡]Department of Materials Science and Engineering, Shenyang University of Chemical Technology, Shenyang 110142, China

S Supporting Information

ABSTRACT: Recently, the chemo-photothermal synergistic therapy has become a potential method for cancer treatment. Herein, we developed a multifunctional nanomaterial for chemo-photothermal therapeutics based on silica and graphene core/shell structure (SiO$_2$@GN) because of the ability of GN to convert light energy into heat. Serum protein was further modified onto the surface of GN (SiO$_2$@GN-Serum) to improve the solubility and stability of GN-based nanoparticles in physiological conditions. The as-synthesized SiO$_2$@GN-Serum nanoparticles (NPs) have been revealed to have high photothermal conversion efficiency and stability, as well as high storage and release capacity for anticancer drug doxorubicin (SiO$_2$@GN-Serum-Dox). The therapeutic efficacy of SiO$_2$@GN-Serum-Dox has been evaluated in vitro and in vivo for cervical cancer therapy. In vitro cytotoxicity tests demonstrate that SiO$_2$@GN-Serum NPs have excellent biocompatibility. However, SiO$_2$@GN-Serum-Dox NPs show higher cytotoxicity than SiO$_2$@GN-Serum and free Dox under irradiation with NIR laser at 1.0 W/cm^2 for 5 min owing to both SiO$_2$@GN-Serum-mediated photothermal ablation and cytotoxicity of light-triggered Dox release. In mouse models, the tumor growth is significantly inhibited by chem-photothermal effect of SiO$_2$@GN-Serum-Dox. Overall, compared with single chemotherapy or photothermal therapy, the combined treatment demonstrates better therapeutic efficacy. Our results suggest a promising GN-based core/shell nanostructure for biomedical applications.

KEYWORDS: graphene, silica, serum protein, drug delivery, photothermal therapy, synergistic effect, cancer therapy
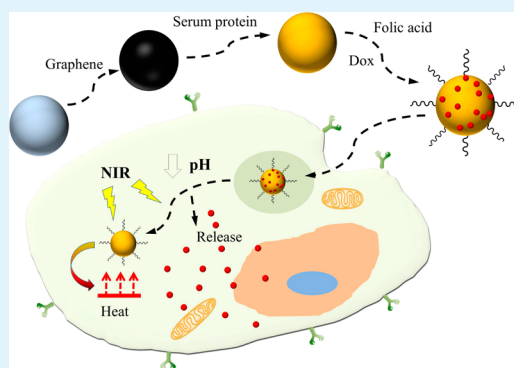
1. INTRODUCTION

Within the past decade, the main treatment of cancer therapy has been relying on single therapy of chemical drugs. Although the cancer cells can be killed efficiently, the normal tissue cells would also be damaged seriously during the treatment, resulting in an unnecessary harm to patients, because of the non-specificity of the chemotherapy. Recently, photothermal therapy, which is based on the principle of converting light energy into heat, has attracted increasing interest as a potentially effective treatment on tumor necrosis. Compared with traditional cancer therapies, photothermal therapy is noninvasive and targeted, which shows the great potential on cancer therapy. Currently, several kinds of nanomaterials have shown the encouraging photothermal therapeutic effects in vitro and in vivo, such as noble metal nanomaterials, semiconductor nanomaterials, and carbon-based nanomaterials.[1−4] In order to enhance the therapeutic efficacy, many multifunctional nano-materials, which combine hyperthermia with chemotherapeutic agents, have been developed.[5−7] Most of the multifunctional nanomaterials have been prepared based on several noble metals, Au and Pt nanomaterials, supported on the silicon substrate[8,9] after Halas's group first applied a coating of gold nanoshells on solid silica spheres for tumor ablation.[10] In these

materials, the noble metal nanomaterials can kill cancer cells by employing hyperthermia and improve the sensitivity of chemotherapy. Besides, the silica spheres can be finely engineered into different structures.[11−13] Although the silica/ noble metal nanomaterials show synergistic effects in cancer therapy, some important limitations still hinder their wide applications. For example, the traditional noble metal nano-materials (Au nanorods, Pd nanoplates) show great perform-ance in photothermal therapy, but the high cost and low photostability have limited their practical applications.[1,14] To meet the development of cancer therapy, overcoming these difficulties will surely become the focus of future research.

Graphene nanosheet (GN) and its derivatives, graphene oxide (GO), have attracted tremendous attention in nano-medicine as drug, protein, gene delivery, and efficient photosensitizer for photothermal therapy in vitro and in vivo[15−21] due to its good biocompatibility, unique structure, and low cost. For instance, the GO-based drug delivery system[19] and the GN-based multifunctional nanohybrids for

imaging and chem-photothermal therapy[20,21] have been fabricated and used to suppress the tumor growth. However, all these reports exploited the large surface area of GO and GN nanosheets, which can load drug and other functional nanoparticles for the tumor treatment. On the other hand, the flexibility of the GN/GO sheet due to the single layer and open porous structure makes it highly suitable to be the shell materials for encapsulating NPs. Hitherto, several reports have demonstrated for encapsulating NPs or macromolecules in GN/GO sheet to form functional composites. The prepared core/shell nanocomposites have shown good properties in energy conversion, storage devices, sensors, and cancer therapy. Especially in cancer therapy, the encapsulation of nanographene oxide (NGO) not only decreased the cytotoxicity of CTAB-coated AuNRs but also exhibited high photothermal energy conversion efficiency and pH-sensitive, NIR-triggered drug release characteristics.[22] From this point, GN might be a promising substituent for noble metal in fabrication of core/shell nanocomposites. However, there is only one related report about GN-encapsulating gold NPs for cancer therapy[23] as far as we know, even though the light absorption of GN is much higher than GO. Most likely due to the insolubility of GN greatly limits its biomedical applications. As we all know, the hydrophobic NPs are generally unstable and poorly dispersed in biological medium.[24]

In order to improve the solubility and stability of GN in physiological conditions, GN is usually functionalized by polyethylene glycol.[25] Recent studies have shown that modification of nanomaterials with biological molecules is a promising route to prepare biocompatible nanomaterials with enhanced solubility and reduced cytotoxicity.[26] In comparison with synthetic polymers, the use of natural biological molecules such as proteins is advantageous due to their biological compatibility, wide availability and great varieties in chemical structures. Some studies have shown that the surface of NPs modified with some proteins such as bovine serum protein has a strong antiadsorption property.[27] Adsorption of serum protein onto the surface of nanomaterials will enhance the dispersibility of NPs.[28]

In this paper, we reported the synthesis and characteristics of multifunctional nanoplatform for chemo-photothermal therapeutics based on SiO₂ and GN core/shell structure (Scheme 1). The negatively charged GN was assembled to the surface of

the positively charged SiO₂ NPs through electrostatic interactions, and the resulted nanocomposites were further modified with serum proteins. The selection of SiO₂ NPs as core will not only enhance the transportation of loaded GN into the cancer cells considering the enhanced endocytosis property of the SiO₂ NPs at the size of around 100 nm but also suggest many possibilities in designing the SiO₂@GN NPs by the controllable preparation of the core structure. The coated GN as a shell material simultaneously processes photothermal conversion ability and drug loading capacity. Most importantly, the modified serum proteins on the surface of GN will significantly improve the dispersibility and biocompatibility of the GN-based core/shell NPs. Meanwhile, the modified protein can be used as multifunction platform to load the anticancer drug Dox and immobilize the targeting molecules of folic acid that is a fully characterized ligand whose receptor is overexpressed in various tumor cells. The developed nanocomposites show low cytotoxicity, high photothermal stability, pH and heat-responsive drug release. The Dox-loaded nanocomposites can effectively ablate tumor cells under the illumination of the near-infrared laser. All the results indicate that the combination of chemotherapy and photothermal therapy could be a more effective way to destroy cancer cells than chemotherapy or photothermal therapy alone. Our work not only expands the application of GN as a shell material in biological system but also provides a possible method in preparation of different SiO₂@GN nanocomposites by engineering the structure of SiO₂ NPs.

2. EXPERIMENTAL SECTION

Chemicals and Reagents. All chemicals were used as received without further purification. All solutions were freshly prepared with deionized water from a Millipore Milli-Q system. Graphite powder, (3-aminopropyl) triethoxysilane (ATPES), folic acid (FA) and N-(3-dimethylamino propyl-N′-ethylcarbodiimide) hydrochloride (EDC•HCl) were purchased from Aladdin Reagent Co. Tetraethyl orthosilicate (TEOS) was purchased from Beijing Chemicals Co. Sodium dodecyl benzenesulfonate (SDBS) was purchased from Xilong Chemical Co. Doxorubicin hydrochloride (Dox) was purchased from Beijing Huafeng United Technology Co. N-hydroxysuccinimide (NHS) was purchased from J&K Chemical Co. Dimethyl sulfoxide (DMSO) and 3-(4,5-dimethylthiazol-2-yl)-2,5-di-pheny-ltetrazolium bromide (MTT) were purchased from Sigma. Dulbecco's modified eagle medium (DMEM), penicillin, fetal bovine serum (FBS), and streptomycin were purchased from Beijing Dingguo Biotechnology Co. Other reagents were purchased from Beijing Chemicals Co. Phosphate buffered saline (PBS) purchased from Invitrogen (10010) was used as a balanced salt solution in cell culture. PBS used in other experiments was prepared by mixing stock solutions of NaH₂PO₄ and Na₂HPO₄.

Characterization. Transmission electron microscopy (TEM) was performed on an H-600 electron microscope (Hitachi, Japan) operated at 75 keV. UV−vis absorption spectra were measured on LAMBDA 25 spectrometer (PerkinElmer). Fourier transform infrared (FTIR) spectra were measured on Vertex 70 FTIR spectrometer (Bruker Co., German). The X-ray photoelectron spectroscopy (XPS) measurements were performed on an ESCALAB 250 X-ray photoelectron spectrometer with a monochromated X-ray source (Al$_{K\alpha}$hν = 1486.6 eV). Zeta potential of the nanocomposites was determined using a dynamic light scattering

Scheme 1. Schematic representation of multifunctional SiO₂@GN-Serum NPs for chemo-photothermal therapy
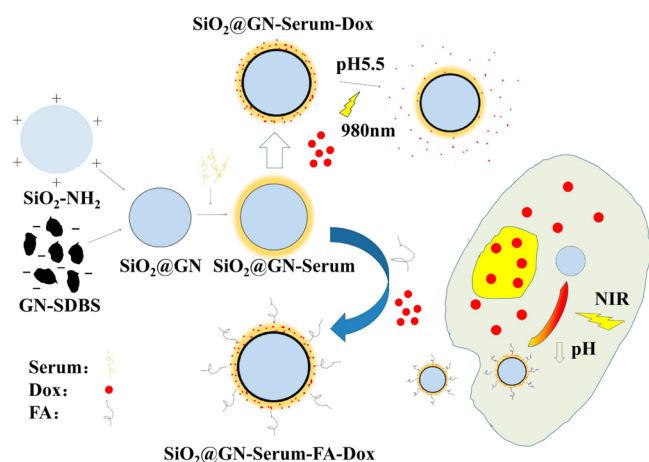
(ZEN 3600, Malvern Instrument, UK). The laser was exported using a power density of 1.0 W/cm^2 (Changchun New Industries Optoelectronics Technology, China). The temperature of the solution was monitored using a digital thermometer with a thermocouple probe (Pyrometer Instrument Company, USA). The cells were imaged using a confocal laser scanning fluorescence microscope (CLSM, Leica TCS SP2, Leica Microsystems, Mannheim, Germany).

Synthesis of SiO$_2$@GN-Serum nanoparticles. Graphene oxide (GO) was prepared by a modified Hummers' method.[29] Briefly, the mixture of graphite flakes (0.3 g) and KMnO$_4$ (3.0 g) was added into the mixed acid of H$_2$SO$_4$/H$_3$PO$_4$ (36 mL/4 mL). After heating to 50 °C, the solution was stirred for 20 h, and then was cooled to the room temperature. The excess H$_2$O$_2$ was added to terminate the reaction. The obtained GO was centrifuged at 12000 rpm for 30 min to remove the solution, and washed in succession with 30% HCl, water and ethanol, respectively. In order to prepare the negatively charged GN solution, 16 mg of SDBS was added into 32 mL of GO solution (0.25 mg/mL) under stirring. After 30 min, the solution was heated to 98 °C, and then 11.2 μL of hydrazine solution and 128 μL of ammonia solution (25%) were added into the GO solution and reacted in refluxing conditions for 1 h. When the color of the solution was changed to dark, the solution was centrifuged at 12000 rpm for 30 min to remove the excess SDBS, and the precipitate was redispersed in water and dialyzed for 3 days. Finally, the SDBS-modified GN (SDBS-GN) was prepared by violent ultrasonication for 7 h.

Positively charged SiO$_2$ NPs were prepared by Stöber method.[30] First, 1.2 mL of ammonia was added into 250 mL of ethanol under stirring and kept for 5 min. Then, 20 mL of TEOS was added dropwise. After stirring for 24 h at room temperature, the solution was centrifuged and washed three times with ethanol and water. Finally, SiO$_2$ NPs were dried at 60 °C in a vacuum drying oven (DZF-6050, Shanghai Jinghong Instrument Co., Ltd., China) overnight. To synthesize amino-modified SiO$_2$ NPs (SiO$_2$−NH$_2$ NPs), 8 mL of 1 wt % SiO$_2$ solution and 0.2 mL of ATPES were added into 20 mL of isopropanol and ultrasonicated for 30 min. Then, the solution was heated to 60 °C and stirred for 6 h. After centrifuging and washing several times, SiO$_2$−NH$_2$ NPs were dried at 60 °C in a vacuum drying oven overnight.

The SiO$_2$@GN-Serum NPs were synthesized easily by self-assembly method. In a typical experiment, 6 mg of SiO$_2$−NH$_2$ NPs was added into 4 mL of water and ultrasonicated for 1 h. Then, 200 μL of 1 mg/mL GN-SDBS solution was added dropwise and ultrasonicated for 1 h to get the GN-coated SiO$_2$ NPs (SiO$_2$@GN NPs). The as-prepared SiO$_2$@GN NPs were obtained after centrifuging and washing. Then, 6 mg of SiO$_2$@GN NPs were dispersed in the solution of FBS under ultrasonication. After 30 min, the protein was immobilized on the surface of SiO$_2$@GN NPs. The as-prepared SiO$_2$@GN-Serum NPs were collected by centrifugation at 10000 rpm for 10 min and washed with water for three times.

To conjugate FA, 1.2 mg of FA was dissolved in 5 mL of PBS solution (pH 5.6). Then, EDS/NHS with 2.5 mg/1.5 mg was added into the above solution. After reaction at room temperature for 30 min, the pH of the solution was adjusted to 7.4 with NaOH, and 6 mg of SiO$_2$@GN-Serum NPs was added into the solution. After stirring at room temperature for 5 h, the mixture was centrifuged, and the supernatant was removed. After washing several times with water to remove

excess reactant, FA- conjugated SiO$_2$@GN-Serum NPs were obtained.

Measurement of Photothermal Performance. To measure the photothermal performance of the SiO$_2$@GN-Serum NPs, 0.5 mL of the sample solution was added into the quartz cuvette and irradiated with the 980 nm laser at a power density of 1.0 W/cm^2. In the experiment, the samples with different concentrations (i.e., 0, 0.5, 1, 2, and 4 mg/mL) were exposed to the laser irradiation for 10 min, and the temperature of the solution was recorded every 10 s. To detect the thermal stability of SiO$_2$@GN-Serum NPs, the samples were cyclically irradiated for 5 min each time, and the temperature was recorded every 20 s.

Loading and Release of Dox. To load Dox, 4 mg of SiO$_2$@GN-Serum NPs was mixed with 30 mL of 0.1 mg/mL Dox in PBS solution (pH 8.0) and stirred overnight in dark. After removing the free Dox by centrifuging and washing several times, the Dox loaded SiO$_2$@GN-Serum NPs was obtained. To evaluate the Dox-loading efficiency (DLE), the content of the original and residual Dox in the supernatant was determined by UV−vis measurements at 482 nm with reference to the standard curve (Supporting Information Figure S1), which was constructed by measuring the absorbance of Dox solutions with different concentrations at 482 nm using a UV−vis spectrometer. The DLE was calculated by eq 1

$$DLE\% = \frac{O_{Dox} - R_{Dox}}{O_{Dox}} \times 100\% \tag{1}$$

where O_{Dox} and R_{Dox} are the contents of the original and residual Dox solution, respectively. In our work, the weight of O_{Dox} and R_{Dox} is 3 mg and 0.3 mg, respectively, which was quantitatively analyzed by UV−vis spectra at the wavelength of 482 nm to the characteristic absorption of free Dox. According to eq 1, the loading efficiency of Dox could reach 90%.

To research the controlled release of Dox, the Dox-loaded SiO$_2$@GN-Serum NPs (1.0 mg) were dispersed in PBS (1 mL, pH 7.4 or 5.0) and shaken at 37 °C and 150 rpm. At selected time intervals, aliquots of PBS (1 mL) were taken out by centrifugation to test the concentration of released Dox by UV−vis measurements at 482 nm and fresh PBS (1 mL) was added to the tube containing the Dox-loaded SiO$_2$@GN-Serum NPs. All the data have been recorded for 60 h.

Cell Viability Assay. The cell viability was measured by the methyl thiazolyl tetrazolium (MTT) assay. HeLa cells were cultured in DMEM containing 10% fetal bovine serum (FBS), 100 units/mL penicillin, and 100 mg/mL streptomycin in a humidified incubator at 37 °C and 5% CO$_2$. Prior to assay, HeLa cells were seeded in a 96-well plate at a density of 1 × 10^4 cells/well and cultured in 5% CO$_2$ at 37 °C for 24 h. After washing three times with PBS, the cells were either exposed to SiO$_2$@GN-Serum-FA NPs dispersed in the fresh culture medium at different concentrations (i.e., 0, 20, 40, 80, 160, 320, 640, and 1280 μg/mL) or exposed to free Dox (10 μg/mL), SiO$_2$@GN-Serum-FA NPs (1000 μg/mL) and SiO$_2$@GN-Serum-FA-Dox NPs (1000 μg/mL, the concentration of Dox was 10 μg/mL), respectively, in the culture medium for 24 h. For the chemo-photothermal assay, the cells were irradiated by NIR laser at a power density of 1.0 W/cm^2 for 10 min. Then, the nanoparticles contained culture medium were removed and 0.1 mL of 0.5 mg/mL MTT solution was added into each well, following incubated for 4 h at 37 °C in the presence of 5% CO$_2$. At the end of the incubated time, the

culture medium was removed and 100 μL of DMSO was added to dissolve the formazan crystals. Finally, the spectrophotometric absorbance of the formazan was measured using a microplate reader at 570 nm.

Confocal Fluorescence Imaging Analysis. Before the confocal microscopy study, HeLa cells were seeded in a 20 mm tissue culture dish (NEST Biotech Co., Ltd., China) and cultured in DMEM containing 10% FBS, 100 units/mL penicillin, and 100 mg/mL streptomycin in a humidified incubator at 37 °C and 5% CO_2 for 24 h. The cells were washed three times with PBS, followed by incubation with 800 μL of SiO$_2$@GN-Serum-FA NPs (1000 μg/mL) or SiO$_2$@GN-Serum-FA-Dox NPs (1000 μg/mL, the concentration of Dox was 10 μg/mL) solution in DMEM culture medium at 37 °C and 5% CO_2 for 24 h. For thermal therapy, corresponding culture dishes were irradiated with laser after incubated for 24 h. Then, all groups were washed three times using PBS and stained with 2 μg/mL of calcein AM in PBS for 30 min. Finally, the living cells were imaged using a confocal laser scanning fluorescence microscope with 10 × objective. The calcein AM could be excited at 488 nm and observed through a 500−550 nm emission band-pass.

Targeting Ability Evaluation in Different Cells. Before the confocal microscopy study, HeLa cells (tumor cell) and 293T cells (normal cell) were respectively seeded in the 20 mm tissue culture dishes (NEST Biotech Co., Ltd., China) and cultured in DMEM containing 10% FBS, 100 units/mL penicillin, and 100 mg/mL streptomycin in a humidified incubator at 37 °C and 5% CO_2 for 24 h. After the cells were washed, 800 μL of SiO$_2$@GN-Serum-FA NPs (500 μg/mL) or SiO$_2$@GN-Serum-FA-Dox NPs (500 μg/mL) were added into the cell culture dishes, and the cells were cultured in DMEM culture medium at 37 °C and 5% CO_2 for 5 h. All groups were then carefully washed with PBS for three times, and the cells were imaged using a confocal laser scanning fluorescence microscope with excitation at 488 nm.

***In Vivo* Photothermal Ablation of Cancer Cells.** Animal care and handing procedures were conducted in conformity with national guidelines and with approval of the regional ethics committee for animal experiments. The U14 cells (5×10^6) were harvested, suspended in PBS (10 mL), and injected subcutaneously into the left shoulder of each female Balb/c mouse at the injection amount of 0.1 mL/animal. The mice were treated when the tumor volumes approached 40−50 mm^3. Then 12 mice were randomly divided into 4 groups (n=3 per group), and saline solution (Group I), free Dox (Group II, 10.0 μg/mL), SiO$_2$@GN-Serum-FA+IR (Group III, 500 μg/mL) and SiO$_2$@GN-Serum-FA-Dox+IR (Group IV, 500 μg/mL, and the concentration of Dox was 10.0 μg/mL) were locally injected into the tumors. After 2 h of injection, an 980 nm continuous-wave NIR laser was used to irradiate tumors at a power density of 1.0 W/cm^2 for 5 min. The tumor sizes were measured by a caliper every third day and calculated as the volume V=(tumor length) × (tumor width)^2/2. Relative tumor volumes were calculated as V/V_0, where V_0 was the tumor volume when the treatment was initiated.

3. RESULTS AND DISCUSSION

Characterization of SiO$_2$@GN-Serum NPs. The SiO$_2$@GN NPs was designed to deliver drug for synergistic chemophotothermal therapy of cancer cell, and the detailed synthesis is shown in Scheme 2. The SiO$_2$@GN nanostructures were synthesized by electrostatic interactions between GN and SiO$_2$

Scheme 2. Procedure for the preparation of SiO$_2$@GN NPs
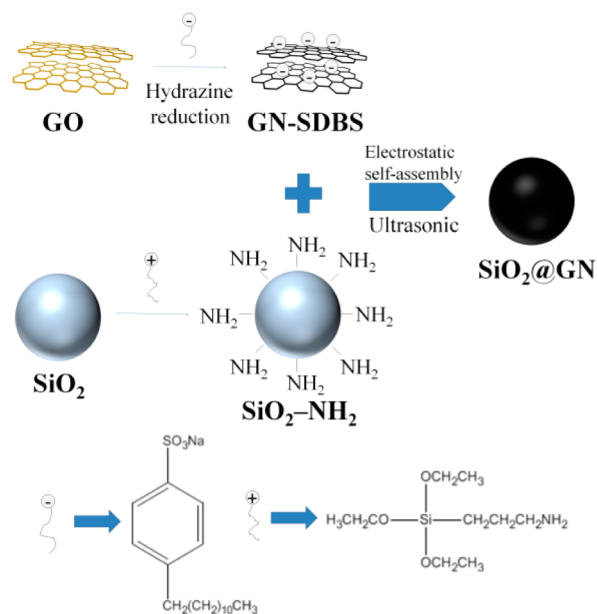
NPs. First, GO was prepared by improved Hummers' method.[29] To obtain the negatively charged GN, GO was reduced with hydrazine in the presence of SDBS.[31] Meanwhile, SiO$_2$ NPs was synthesized by Stöber method, and the amino groups were immobilized on the negatively charged surface of SiO$_2$ NPs through the hydrolysis of ATPES.[30,32] Finally, the negative GN-SDBS was covered on the surface of the positive SiO$_2$−NH$_2$ NPs through the electrostatic interactions. The sequential preparations were first characterized by zeta-potential and UV−vis measurements, respectively. The mean zeta-potentials of the as-prepared GN-SDBS and amino-functionalized SiO$_2$ NPs were −43 ± 1.2 and +27.9 ± 0.8 mV, respectively (Table 1). After mixing the negatively charged

Table 1. Zeta Potentials of GN-SDBS, SiO$_2$−NH$_2$, SiO$_2$@GN. and SiO$_2$@GN-Serum NPs Dispersed in Water

sample	GN-SDBS	SiO$_2$−NH$_2$	SiO$_2$@GN	SiO$_2$@GN-Serum
zeta potential (mV)	−43 ± 1.2	+27.9 ± 0.8	−14.6 ± 0.8	−24.8 ± 0.4

GN-SDBS and positively charged SiO$_2$ NPs, GN-SDBS was adsorbed onto the surface of SiO$_2$ NPs by electrostatic interactions and the zeta-potential of the resulted SiO$_2$@GN NPs was about −14.6 ± 0.8 mV. In Figure 1, the UV−vis absorption spectrum of GO shows a strong absorption peak at 230 nm (a), corresponding to $\pi \rightarrow \pi*$ transition of the aromatic C−C bands.[29] During the reduction process, the absorption peak of GO at 230 nm shifts to 255 nm (b), indicating that the GO has been successfully reduced to GN because of the considerable reduction capability of hydrazine at high temperature. Meanwhile, the UV−vis absorption spectrum of the GN-SDBS also shows the characteristic absorption peak of SDBS at 224 nm (b and c), indicating that SDBS has been successfully grafted on the surface of GN. The characteristic absorption peak of GN can be found easily at the absorption curve of SiO$_2$@GN NPs at 255 nm, indicating the successful formation of SiO$_2$@GN NPs (d). The structural and
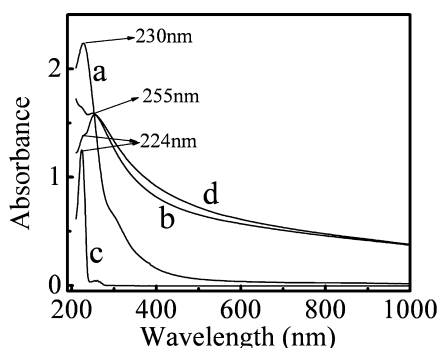
Figure 1. UV−vis absorption spectra of GO (a), GN-SDBS (b), SDBS (c), and SiO$_2$@GN (d) dispersed in aqueous solution.

morphological characterization was observed by TEM and high-resolution TEM (HRTEM) measurements. As shown in Figure 2A, GO was successfully prepared with the ripped and
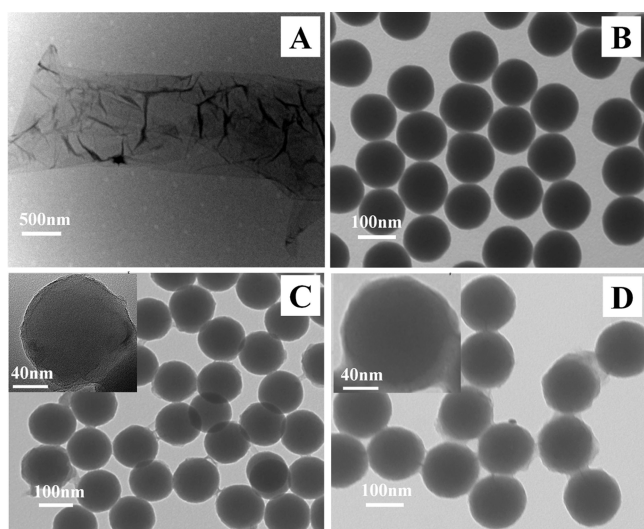

Figure 2. TEM images of (A) GN, (B) SiO$_2$ NPs, (C) SiO$_2$@GN NPs, and (D) SiO$_2$@GN-Serum NPs. Inset is the HRTEM of (E) SiO$_2$@GN NPs and (F) SiO$_2$@GN-Serum NPs.

layered structure (A). TEM image shows that the sphere SiO$_2$ nanoparticles have been prepared using the common base-catalyzed Stöber method (Figure 2B). As expected, these spheres are well monodisperse and nearly uniform in dimension with an average diameter of around 130 ± 4 nm (Figure S2A). After assembly of the two opposite charged GN and SiO$_2$ NPs, folds can be observed on the surface of the spherical particles (Figure 2C), which is associated with the presence of flexible and ultrathin GN. In most cases, SiO$_2$ nanoparticles were singly encapsulated in GN shells. The corresponding HRTEM image (inset in Figure 2C) shows that an ultrathin GN layer of about 9 nm is clearly evident on the outer surface of the SiO$_2$ NPs. The histogram of particle size distribution of nanoparticles was shown in Figure S2B with the mean particle diameter of 148 ± 6 nm.

To improve the solubility of the as-prepared nanoparticles, GN-coated SiO$_2$ NPs were further modified with serum proteins through hydrophobic interactions. When the SiO$_2$@GN NPs were sonicated in the FBS solution, the hydrophobic groups of the serum proteins could be assembled on the hydrophobic surface of GN, and the hydrophilic groups of

proteins improved the dispersibility of SiO$_2$@GN NPs.[33] After serum protein conjugation to SiO$_2$@GN NPs, trilaminar core−shell nanostructure of SiO$_2$@GN-Serum nanospheres with an inner SiO$_2$ core and outer serum protein highly dispersed on the surface of SiO$_2$@GN NPs was characterized by TEM (Figure 2D). The thickness of the serum protein shell is about 4.5 nm, as measured from HRTEM (inset in Figure 2D). A histogram of particle size distribution of SiO$_2$@GN-Serum NPs shows the narrow size distribution of particles with a mean particle diameter of 157 ± 7 nm (Supporting Information Figure S2C). To further validate the particle size distribution, the dynamic light scattering has been used to count the samples, showing an approximate result (Supporting Information Figure S2E−F) with a diameter of 147.8 ± 27, 176 ± 7, and 187.5 ± 0.2 nm, respectively, for SiO$_2$ NPs, SiO$_2$@GN NPs, and SiO$_2$@GN-Serum NPs dispersed in aqueous solution. To demonstrate the immobilization of serum proteins on the surface of SiO$_2$@GN NPs, we characterized the modification by FTIR spectroscopy (Figure 3A). The peak at 1624 cm^{-1} in the
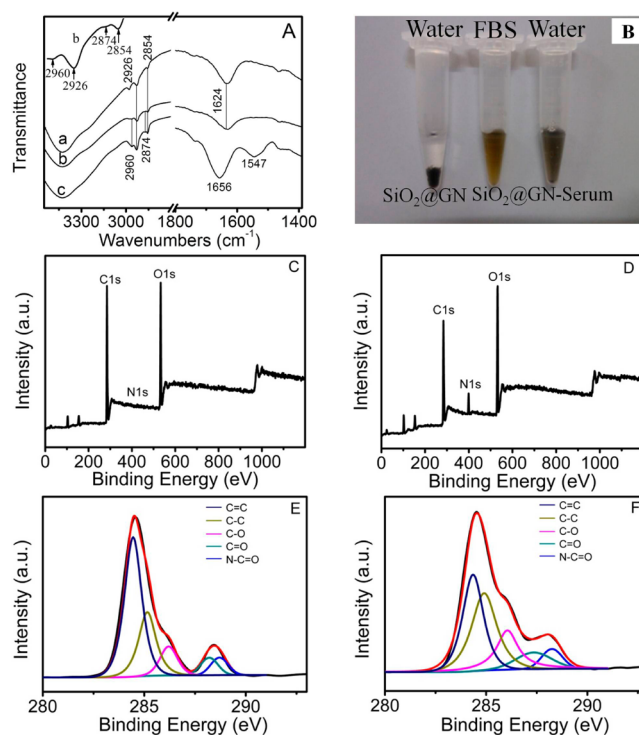

Figure 3. (A) FTIR spectra of SiO$_2$−NH$_2$ (a), SiO$_2$@GN (b), and SiO$_2$@GN-Serum (c). (B) Photograph of SiO$_2$@GN NPs in water, SiO$_2$@GN-Serum NPs in FBS and water after 4 h. XPS survey spectra of (C) SiO$_2$@GN and (D) SiO$_2$@GN-Serum. C 1s spectra of (E) SiO$_2$@GN and (F) SiO$_2$@GN-Serum.

FTIR spectrum of SiO$_2$−NH$_2$ NPs (a) indicates the asymmetrical deformation vibration of NH$_3$$^+$.[34] The bands around 2854 and 2926 cm^{-1} are the symmetric and asymmetric stretching vibration of −CH$_2$ in APTES.[35] After coating by GN-SDBS, the bands at 2874 and 2960 cm^{-1} are observed in the spectrum of SiO$_2$@GN NPs (curve b and the inset at the top left corner of Figure 3A), indicating the symmetric and asymmetric stretching vibration of −CH$_3$ in SDBS.[36] The characteristic absorption of the amide I and amide II bands of proteins at about 1656 and 1547 cm^{-1} that were not observed in the curves of SiO$_2$−NH$_2$ and SiO$_2$@GN NPs, clearly confirms the existence of serum protein in the SiO$_2$@GN-

Serum NPs (c).[37] Obviously, the dispersibility of SiO$_2$@GN-Serum NPs was significantly improved in water or FBS compared with that of the SiO$_2$@GN NPs in water (Figure 3B). Furthermore, the presence of serum proteins on the surface of SiO$_2$@GN NPs was confirmed by X-ray photo-electron spectroscopy (XPS). It can be seen that the full XPS spectra of the composites demonstrate the existence of C, N, and O elements (Figure 3C and D). Here, the presence of serum proteins can be followed by estimating the increase in nitrogen (N) content to 6.0% originating from amino acids of adsorbed proteins. The high resolution carbon (C) 1s spectrum of SiO$_2$@GN NPs (Figure 3E) was deconvoluted into five different peaks arising from C=C (284.7 eV), C−C (285.3 eV), C−O (286.2 eV), C=O (287.4 eV) and N−C=O (288.6 eV).[38,39] By comparison of C 1s peaks of SiO$_2$@GN NPs, it is obvious that the peak intensities of C=O and N−C=O increase, and the peak intensity of C=C significantly reduces after adsorption of serum on the surface of SiO$_2$@GN NPs, indicating the binding of serum proteins to the SiO$_2$@GN NPs (Figure 3F). These XPS results agree well with those of the FTIR spectra, further confirming the presence of serum proteins in the SiO$_2$@GN-Serum NPs.

Photothermal Performance of SiO$_2$@GN-Serum NPs. The strong near-infrared (NIR) absorption of GN suggests that GN can be widely used in photothermal therapy for tumor.[40] To investigate the photothermal conversion efficiency of SiO$_2$@GN-Serum NPs, the aqueous solution dispersions of SiO$_2$@GN-Serum NPs with different concentrations (0−4 mg/mL) were illuminated using 980 nm laser at a power density of 1.0 W/cm^2 as the excellent penetration ability of the 980 nm laser.[41] As shown in Figure 4A, the pure water as blank test only
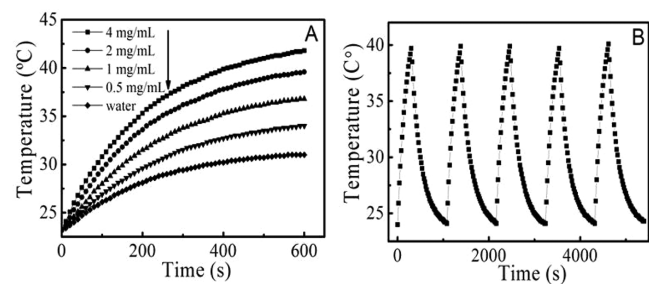

Figure 4. (A) The temperature profiles of aqueous dispersions of SiO$_2$@GN-Serum NPs at different concentrations under NIR light irradiation (980 nm, 1 W/cm^2); (B) Temperature elevation of SiO$_2$@GN-Serum NPs dispersed in 1 mL of PBS solution (4 mg/mL) over five lasers on/off cycles under NIR laser irradiation.

increases by 6 °C from the room temperature, while 0.5 mg/mL of the sample solution increases by 10 °C after irradiation for 10 min. With the increase of the sample concentration (i.e., from 1 to 2, and 4 mg/mL), the temperature of the sample solutions can increase by 14, 17, and 19.5 °C, respectively, in 10 min. Furthermore, we also studied the thermal stability of the SiO$_2$@GN-Serum NPs under the NIR laser irradiation. We recorded the time-dependent temperature of the SiO$_2$@GN-Serum NPs aqueous dispersion upon their irradiation with the NIR laser for 5 min (Laser on), followed by naturally cooling of temperature to room temperature upon the switch off the NIR laser (Laser off). This cycle was repeated five times in order to investigate the photostability of SiO$_2$@GN-Serum NPs (Figure 4B). We did not observe any noticeable attenuation in the thermal conversion efficiency of the SiO$_2$@GN-Serum NPs

after five cycles of laser irradiation (Figure 4B), which is superior to the reported Au nanostructures.[42] The normal photothermal conversion efficiency and the well thermal stability indicate that the SiO$_2$@GN-Serum NPs could be used well in the photothermal therapy.

In Vitro Dox Delivery. On the other hand, it was reported that GN and protein could be used for loading Dox through $\pi−\pi$ stacking or electrostatic interactions.[15,43] Obviously, the SiO$_2$@GN-Serum NPs could also be applied for drug delivery. As we all know that the solubility of Dox increases with the declining of pH.[44,45] In our experiments, we loaded the Dox on the SiO$_2$@GN-Serum NPs in PBS solution at pH 8.0. As shown in Figure 5A, when the SiO$_2$@GN-Serum NPs were incubated
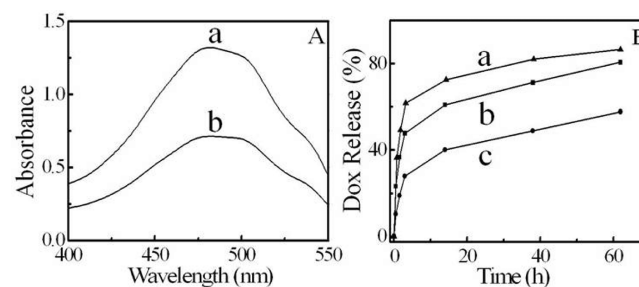

Figure 5. (A) The UV−vis spectra of Dox solution before (a) and after nanocomposites loading (b). (B) The release profiles of Dox from Dox-loaded SiO$_2$@GN-Serum NPs at pH 5.5 with (a) or without (b) the irradiation (1.0 W/cm^2, 980 nm), and the release profile of Dox at pH 7.0 (c).

with Dox solution overnight, the absorption of the Dox supernatant at 482 nm decreases, indicating that some of the free Dox have been loaded on the SiO$_2$@GN-Serum NPs. Also, the loading efficiency of Dox on the SiO$_2$@GN-Serum NPs was 90%, which was calculated by measuring the concentration of unbound drug according to the characteristic absorption of free Dox in the UV−vis spectra (Figure 5A), and the drug loading content was 0.675 mg Dox mg^{-1} SiO$_2$@GN-Serum NPs. Meanwhile, we studied the release of Dox in different conditions. The release amount of Dox was determined under different conditions by measuring the absorption of Dox at 482 nm. It was reported that the tumor microenvironment could be stabilized at a mildly acidic environment with a pH 5.8−7.1 and the intracellular environment could be more acidic with a pH 5.0.[46,47] To study the controllable release of the drug from the SiO$_2$@GN-Serum NPs, the release rate of Dox at pH 5.5 and 7.0 was measured. As shown in Figure 5B, the Dox release was quick within the first 4 h in PBS, and thereafter, it became a slow and continuous process. The release rate of Dox at pH 5.5 (b) was nearly twice greater than that at pH 7.0 (c). The release rate could be further improved from 80% to 90% under the irradiation (a). These results indicate that the acidic environment and the photothermal effect improve the release of Dox. It means that the SiO$_2$@GN-Serum NPs could be very efficient in the acid and NIR-triggered chemotherapy.

Cytotoxicity and Cellular Uptake Study of SiO$_2$@GN-Serum-FA NPs In Vitro. To enhance the targeting capability of the particles to cancer cells, FA ligands were covalently conjugated with the protein of SiO$_2$@GN-Serum NPs. The carboxyl-groups in the FA could be conjugated with the amino-groups in the proteins.[48] The UV−vis absorption spectrum shows the characteristic absorption of FA at 280 nm for the

SiO_2@GN-Serum-FA NPs dispersion even after the particles were fully washed several times (Figure 6A), indicating the
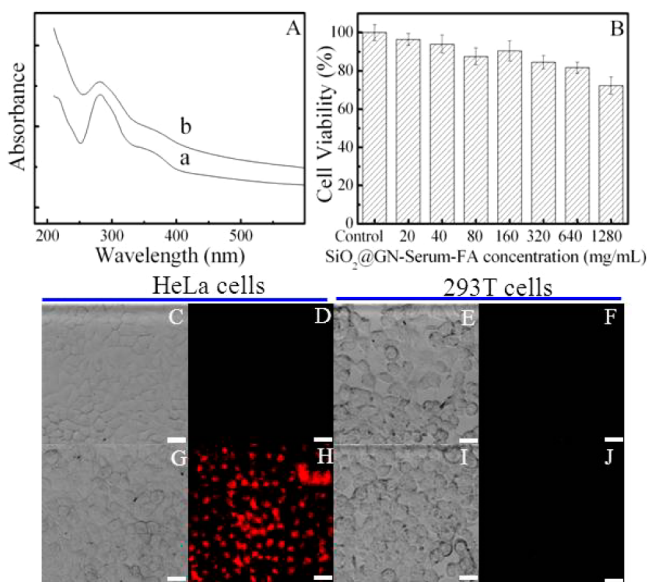

Figure 6. (A) UV−vis absorption spectra of FA (a) and SiO_2@GN-Serum-FA NPs (b) dispersed in aqueous solution. (B) The viability of HeLa cells incubated with the SiO_2@GN-Serum-FA NPs at different concentrations; Confocal microscopy images of HeLa cells and 293T cells incubated with SiO_2@GN-Serum-FA (C−F) and SiO_2@GN-Serum-FA-Dox (G−J) for 5 h. C, E, G, and I are the corresponding bright field images of fluorescent images D, F, H, and J. Red: Dox. Bar = 30 μm.

successful conjugation of FA to the SiO_2@GN-Serum NPs. The conjugation of FA is also indicated from the change of carbon atom percentage (Supporting Information Figure S3A). It can be seen that the percentage of the carbon atom content and the integrated area of the C═C peak (284.3 eV) for the SiO_2@GN-Serum-FA NPs (Supporting Information Figure S3B) increase in comparison with those for the SiO_2@GN-Serum NPs (Figure 3D). Further evidence of the surface-immobilized FA is provided by the enhancement of the C═N peak at 400.1 eV (Supporting Information Figure S3D). However, the C−N peak at 390.1 eV is major peak for the SiO_2@GN-Serum NPs (Supporting Information Figure S3C).

To evaluate the biocompatibility of the particles in vitro, the viability of the HeLa cells incubated with SiO_2@GN-Serum-FA NPs were determined by MTT assay. The MTT assay is a colorimetric assay for assessing cell viability, which could represent a viable parameter for reporting metabolic activity. As shown in Figure 6B, the cell viability was even maintained at about 80% with the concentration of the SiO_2@GN-Serum-FA NPs as high as 1280 μg/mL. The results indicate that the SiO_2@GN-Serum-FA NPs have low cytotoxicity and good biocompatibility.

To evaluate whether FA-conjugated particles facilitate the efficiency of cell uptake by HeLa cells because of receptor-mediated endocytosis, cellular uptake of the modified particles was observed using confocal microscopy. HeLa cells (FA+) and 293T cells (FA-) were chosen as target cells and control cells, respectively. Dox was loaded onto the samples to observe the cellular uptake of SiO_2@GN-Serum-FA NPs. As shown in Figure 6C−J, the very little red fluorescence was observed in the two types of cells after incubation with SiO_2@GN-Serum-FA NPs (Figure 6D and F). In contrast, the red fluorescence of Dox was clearly observed in HeLa cells after incubation with SiO_2@GN-Serum-FA-Dox NPs for 5 h (Figure 6H), indicating that nanoparticles have been uptaken by the cells. However, the fluorescence in 293T cells (normal cells) was negligible after incubation with SiO_2@GN-Serum-FA-Dox NPs (Figure 6J), implying a negligible cellular uptake due to the low expression level of FA receptors for 293T cells. It can be concluded that the as-prepared nanocomposites can be effectively taken up by HeLa cells.

The Chemo-Photothermal Synergistic Therapy. To investigate therapeutic efficacy of the Dox-loaded SiO_2@GN-Serum-FA NPs in vitro, the comparative studies on inhibiting tumor cells effectiveness have been conducted (Figure 7A). As expected, the cellular viability only decreased to about 82% at an incubation concentration of SiO_2@GN-Serum-FA NPs up to 1000 μg/mL without irradiation. After irradiation, the viability of the cells incubated with SiO_2@GN-Serum-FA NPs was less than 50%. The differences can be explained by the photothermal effect of SiO_2@GN-Serum-FA NPs. After incubation of cells with SiO_2@GN-Serum-FA-Dox NPs, the cell viability was higher than that of the cells treating with free Dox at an equivalent concentration of 10 μg/mL and lower than that of the cells treating with SiO_2@GN-Serum-FA NPs without irradiation. We considered that the result was
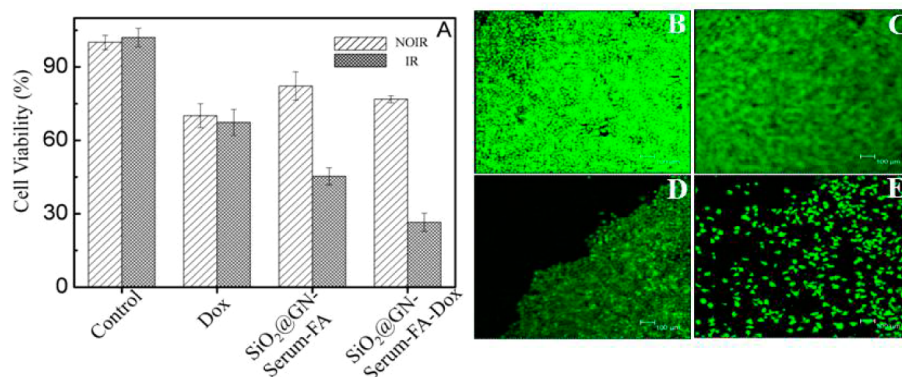

Figure 7. (A) Viability of HeLa cells incubated with PBS as control, free Dox, SiO_2@GN-Serum-FA NPs, and SiO_2@GN-Serum-FA-Dox NPs with and without NIR irradiation at 1 W/cm²; Confocal images of HeLa cells incubated with (B) DMEM medium, (C, D) SiO_2@GN-Serum-FA NPs, and (E) SiO_2@GN-Serum-FA-Dox NPs dispersed in DMEM for 24 h at 37 °C without (B, C) and with (D, E) NIR irradiation at 1 W/cm² for 5 min.
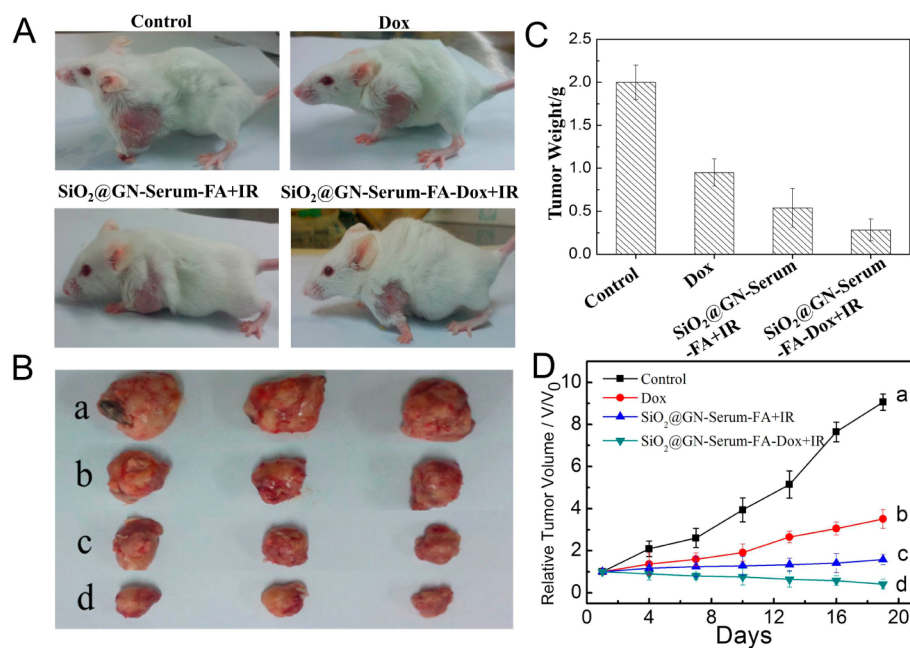
Figure 8. (A) Representative photos of tumors on mice after various treatments indicated. (B) Photograph of tumors from (a) Control group, (b) Dox group, (c) SiO₂@GN-Serum-FA+IR group, and (d) SiO₂@GN-Serum-FA-Dox+IR group. (C) Tumor weights of each group after excision. (D) Tumor growth curves of different groups after treatment. The tumor volumes were normalized to their initial sizes.

attributed to incomplete release of Dox from SiO₂@GN-Serum-FA-Dox NPs. When the SiO₂@GN-Serum-FA-Dox NPs were endocytosed into cells, the acidic environment in the cell and the enzymatic degradation of the protein in the SiO₂@GN-Serum-FA-Dox NPs accelerate the release of Dox. When we treated these samples under the irradiation, the cytotoxicity of the control group and the free Dox group did not change significantly compared with the groups without the irradiation. On the contrary, the cytotoxicity of the SiO₂@GN-Serum-FA NPs and the SiO₂@GN-Serum-FA-Dox NPs with irradiation increased double and triple compared with the same groups without irradiation. Obviously, the SiO₂@GN-Serum-FA-Dox NPs with the laser irradiation shows the highest cytotoxicity in all groups, which is attributed to the photothermal effect and heating-triggered drug release. From the results, we claim that the SiO₂@GN-Serum-FA-Dox NPs can be used in the chemo-photothermal synergistic therapy.

To further verify the chemo-photothermal synergistic therapy of the composites, we used scanning confocal fluorescence microscopy to observe the viability of HeLa cells (Figure 7B–E). The living cells could be stained with calcein AM. We investigated the therapy ability of the SiO₂@GN-Serum-FA NPs and Dox loaded SiO₂@GN-Serum-FA NPs with or without NIR irradiation. As shown in Figure 7B and C, there is no significant difference between the control group and the SiO₂@GN-Serum-FA NPs group without laser, which further sugguts the well biocompatibility of our material. When HeLa cells were incubated with SiO₂@GN-Serum-FA NPs and exposed to 980 nm laser irradtion at a power density of 1.0 W/cm² for 5 min, the fluorescence of irradiation region disappeared, indicating that the laser irradiation efficiently killed tumor cells (Figure 7D). The results indicate the ability of the SiO₂@GN-Serum-FA NPs on photothermal therapy. Compared with the group of SiO₂@GN-Serum-FA NPs with laser irradiation, the SiO₂@GN-Serum-FA-Dox NPs group with the irradiation further showed high cytotoxicity except the

irridiation area, which was attributed to the release of Dox from SiO₂@GN-Serum-FA-Dox NPs with laser irradiation (Figure 7E). The results suggest an effective chemo-photothermal synergistic therapy based on SiO₂@GN-Serum-FA-Dox NPs.

In Vivo Chemo-Photothermal Therapy. To investigate therapeutic efficacy of the SiO₂@GN-Serum-FA-Dox NPs in vivo, comparative studies of inhibiting tumor effectiveness have been conducted. Twelve female Balb/c mice bearing cervical cancer model were randomly distributed into four groups, that is, control group, Dox group, SiO₂@GN-Serum-FA+IR group and SiO₂@GN-Serum-FA-Dox+IR group. On the 19th day, mice were sacrificed and tumors were excised and weighed. Photographs of the test mice and the tumors in each group after the treatment on the 19th day are shown in Figure 8A and B. The mean tumor weights in each group after the treatment are shown in Figure 8C. The size of tumor was measured every 3 days after treatment and plotted as a function of time in Figure 8D. It was observed that the mice only treated with 0.9% NaCl solution exhibited rapidly increasing tumor volumes and tumor weight. Compared with the control group, there was only a slight inhibition of tumor growth treated with free Dox, indicating the poor efficacy in regressing tumor growth. While for the group treated with the SiO₂@GN-Serum-FA NPs under NIR light, enhanced inhibition of tumor growth was observed. The mean tumor weight in the SiO₂@GN-Serum-FA+IR group (0.74 ± 0.22 g) was smaller than that of the control group (2.0 ± 0.20 g) and free Dox group (1.15 ± 0.16 g), which demonstrates that the SiO₂@GN-Serum-FA can somewhat inhibit tumor growth in vivo under the NIR laser irradiation. It is worth noting that the group treated with SiO₂@GN-Serum-FA-Dox+IR showed significantly enhanced antitumor activity, and a sharp decrease of tumor volume is observed in comparison with the control group, Dox group, and the SiO₂@GN-Serum-FA+IR group (Figure 8D). No tumor regrowth was observed in this group over a course of 19 days. The mean tumor weight in the SiO₂@GN-Serum-FA-Dox

+IR group was 0.28 ± 0.13 g, which was significantly smaller than that of the control group (2.0 ± 0.20 g), Dox group (1.15 ± 0.16 g), and the SiO$_2$@GN-Serum-FA+IR group (0.74 ± 0.22 g), as shown in Figure 8C. These results clearly demonstrate the evidence of synergistic effect of combining photothermal therapy and chemotherapy in tumor growth inhibition based on the SiO$_2$@GN-Serum-FA-Dox NPs in vivo.

4. CONCLUSIONS

In summary, we have synthesized the multifunctional SiO$_2$@GN-Serum NPs and studied the performance of the new material on the photothermal conversion and drug delivery. Our results indicated that the developed nanocomposites showed high photothermal stability, as well as pH and heat-responsive drug release. When the SiO$_2$@GN-Serum-FA-Dox NPs were uptaken into the cell, the release of the Dox was prompted by acidic environment and the NIR irradiation. Meanwhile, the cells could be killed by the released drug and the local heating induced by the photothermal conversion of the SiO$_2$@GN-Serum-FA-Dox NPs under the NIR irradiation. Our results demonstrated the excellence of SiO$_2$@GN-Serum NPs as multifunctional material for chemo-photothermal synergistic therapy compared with individual photothermal therapy or chemotherapy. There is no doubt that SiO$_2$@GN-Serum NPs would be a potential platform for biomedical application.

ASSOCIATED CONTENT

Ⓢ Supporting Information

The corresponding calibration plot for Dox; the histograms of particle size distribution of SiO$_2$ NPs, SiO$_2$@GN NPs, and SiO$_2$@GN-Serum NPs; the XPS survey spectrum of SiO$_2$@GN-Serum-FA. This material is available free of charge via the Internet at http://pubs.acs.org.

AUTHOR INFORMATION

Corresponding Authors
*Phone: +86 431 85262426. Fax: +86 431 85685653. E-mail: jiangxiue@ciac.jl.cn.
*E-mail: guozhuochina@syuct.edu.cn.
Author Contributions
Yuwei Liu and Jing Bai contributed equally.
Notes
The authors declare no competing financial interest.

ACKNOWLEDGMENTS

REFERENCES

(1) Huang, X.; El-Sayed, I. H.; Qian, W.; El-Sayed, M. A. Cancer Cell Imaging and Photothermal Therapy in the Near-Infrared Region by Using Gold Nanorods. *J. Am. Chem. Soc.* **2006**, *128*, 2115−2120.

(2) Niidome, T.; Yamagata, M.; Okamoto, Y.; Akiyama, Y.; Takahashi, H.; Kawano, T.; Katayama, Y.; Niidome, Y. PEG-Modified Gold Nanorods with a Stealth Character for *in Vivo* Applications. *J. Controlled Release* **2006**, *114*, 343−347.

(3) He, S.; Wang, G.-S.; Lu, C.; Liu, J.; Wen, B.; Liu, H.; Guo, L.; Cao, M.-S. Enhanced Wave Absorption of Nanocomposites Based on the Synthesized Complex Symmetrical CuS Nanostructure and Poly(Vinylidene Fluoride). *J. Mater. Chem. A* **2013**, *1*, 4685−4692.

(4) Liu, Z.; Robinson, J. T.; Tabakman, S. M.; Yang, K.; Dai, H. Carbon Materials for Drug Delivery & Cancer Therapy. *Mater. Today* **2011**, *14*, 316−323.

(5) Jiang, Z.; Dong, B.; Chen, B.; Wang, J.; Xu, L.; Zhang, S.; Song, H. Multifunctional Au@mSiO$_2$/Rhodamine B Isothiocyanate Nanocomposites: Cell Imaging, Photocontrolled Drug Release, and Photothermal Therapy for Cancer Cells. *Small* **2013**, *9*, 604−612.

(6) Liu, H.; Chen, D.; Li, L.; Liu, T.; Tan, L.; Wu, X.; Tang, F. Multifunctional Gold Nanoshells on Silica Nanorattles: A Platform for the Combination of Photothermal Therapy and Chemotherapy with Low Systemic Toxicity. *Angew. Chem., Int. Ed.* **2011**, *50*, 891−895.

(7) Hu, B.; Zhang, L. P.; Chen, X. W.; Wang, J. H. Gold Nanorod-Covered Kanamycin-loaded Hollow SiO$_2$ (HSKAu$_{Rod}$) Nanocapsules for Drug Delivery and Photothermal Therapy on Bacteria. *Nanoscale* **2013**, *5*, 246−252.

(8) Fang, W.; Tang, S.; Liu, P.; Fang, X.; Gong, J.; Zheng, N. Pd Nanosheet-covered Hollow Mesoporous Silica Nanoparticles as a Platform for the Chemo-Photothermal Treatment of Cancer Cells. *Small* **2012**, *8*, 3816−3822.

(9) Shen, S.; Tang, H.; Zhang, X.; Ren, J.; Pang, Z.; Wang, D.; Gao, H.; Qian, Y.; Jiang, X.; Yang, W. Targeting Mesoporous Silica-Encapsulated Gold Nanorods for Chemo-Photothermal Therapy with Near-Infrared Radiation. *Biomaterials* **2013**, *34*, 3150−3158.

(10) Hirsch, L. R.; Stafford, R. J.; Bankson, J. A.; Sershen, S. R.; Rivera, B.; Price, R. E.; Hazle, J. D.; Halas, N. J.; West, J. L. Nanoshell-Mediated Near-infrared Thermal Therapy of Tumors under Magnetic Resonance Guidance. *Proc. Natl. Acad. Sci. U. S. A.* **2003**, *100*, 13549−13554.

(11) Fang, W.; Yang, J.; Gong, J.; Zheng, N. Photo- and pH-Triggered Release of Anticancer Drugs from Mesoporous Silica-Coated Pd@Ag Nanoparticles. *Adv. Funct. Mater.* **2012**, *22*, 842−848.

(12) Vivero-Escoto, J. L.; Slowing, I. I.; Wu, C.-W.; Lin, V. S. Y. Photoinduced Intracellular Controlled Release Drug Delivery in Human Cells by Gold-Capped Mesoporous Silica Nanosphere. *J. Am. Chem. Soc.* **2009**, *131*, 3462−3463.

(13) Zhao, Z. X.; Huang, Y. Z.; Shi, S. G.; Tang, S. H.; Li, D. H.; Chen, X. L. Cancer Therapy Improvement with Mesoporous Silica Nanoparticles Combining Photodynamic and Photothermal Therapy. *Nanotechnology* **2014**, *25*, 285701−285709.

(14) Tang, S.; Huang, X.; Zheng, N. Silica Coating Improves the Efficacy of Pd Nanosheets for Photothermal Therapy of Cancer Cells Using near Infrared Laser. *Chem. Commun.* **2011**, *47*, 3948−3950.

(15) Sun, X.; Liu, Z.; Welsher, K.; Robinson, J. T.; Goodwin, A.; Zaric, S.; Dai, H. Nano-Graphene Oxide for Cellular Imaging and Drug Delivery. *Nano Res.* **2008**, *1*, 203−212.

(16) Liu, J.; Fu, S.; Yuan, B.; Li, Y.; Deng, Z. Toward a Universal "Adhesive Nanosheet" for the Assembly of Multiple Nanoparticles Based on a Protein-Induced Reduction/Decoration of Graphene Oxide. *J. Am. Chem. Soc.* **2010**, *132*, 7279−7281.

(17) Liu, J.; Li, Y.; Li, Y.; Li, J.; Deng, Z. Noncovalent DNA Decorations of Graphene Oxide and Reduced Graphene Oxide toward Water-Soluble Metal-Carbon Hybrid Nanostructures via Self-Assembly. *J. Mater. Chem.* **2010**, *20*, 900−906.

(18) Yang, K.; Zhang, S.; Zhang, G.; Sun, X.; Lee, S.-T.; Liu, Z. Graphene in Mice: Ultrahigh *in Vivo* Tumor Uptake and Efficient Photothermal Therapy. *Nano Lett.* **2010**, *10*, 3318−3323.

(19) Wu, H.; Shi, H.; Wang, Y.; Jia, X.; Tang, C.; Zhang, J.; Yang, S. Hyaluronic Acid Conjugated Graphene Oxide for Targeted Drug Delivery. *Carbon* **2014**, *69*, 379−389.

(20) Li, Y.; Liu, J.; Dong, H.; Liu, G.; Hu, H. Engineering of a Pluronic F127 Functionalized Magnetite/Graphene Nanohybrid for Chemophototherapy. *Nanotechnology* **2014**, *25*, 065602−065611.

(21) Wang, Y.; Huang, R.; Liang, G.; Zhang, Z.; Zhang, P.; Yu, S.; Kong, J. MRI-Visualized, Dual-Targeting, Combined Tumor Therapy

Using Magnetic Graphene-Based Mesoporous Silica. *Small* **2014**, *10*, 109−116.

(22) Xu, C.; Yang, D.; Mei, L.; Li, Q.; Zhu, H.; Wang, T. Targeting Chemophotothermal Therapy of Hepatoma by Gold Nanorods/ Graphene Oxide Core/Shell Nanocomposites. *ACS Appl. Mater. Interfaces* **2013**, *5*, 12911−12920.

(23) Bian, X.; Song, Z.-L.; Qian, Y.; Gao, W.; Cheng, Z.-Q.; Chen, L.; Liang, H.; Ding, D.; Nie, X.-K.; Chen, Z.; Tan, W. Fabrication of Graphene-Isolated-Au-Nanocrystal Nanostructures for Multimodal Cell Imaging and Photothermal-Enhanced Chemotherapy. *Sci. Rep.* **2014**, *4*, 6093−6101.

(24) Zhu, M.; Nie, G.; Meng, H.; Xia, T.; Nel, A.; Zhao, Y. Physicochemical Properties Determine Nanomaterial Cellular Uptake, Transport, and Fate. *Acc. Chem. Res.* **2012**, *46*, 622−631.

(25) Robinson, J. T.; Tabakman, S. M.; Liang, Y.; Wang, H.; Sanchez Casalongue, H.; Vinh, D.; Dai, H. Ultrasmall Reduced Graphene Oxide with High Near-Infrared Absorbance for Photothermal Therapy. *J. Am. Chem. Soc.* **2011**, *133*, 6825−6831.

(26) Wang, Y.; Li, Z.; Wang, J.; Li, J.; Lin, Y. Graphene and Graphene Oxide: Biofunctionalization and Applications in Biotechnology. *Trends Biotechnol.* **2011**, *29*, 205−212.

(27) Ji, A. J.; Jiang, Z.; Livson, Y.; Davis, J. A.; Chu, J. X.; Weng, N. Challenges in Urine Bioanalytical Assays: Overcoming Nonspecific Binding. *Bioanalysis* **2010**, *2*, 1573−1586.

(28) Xia, B.; Zhang, W.; Shi, J.; Xiao, S.-j. Engineered Stealth Porous Silicon Nanoparticles *via* Surface Encapsulation of Bovine Serum Albumin for Prolonging Blood Circulation *in Vivo*. *ACS Appl. Mater. Interfaces* **2013**, *5*, 11718−11724.

(29) Marcano, D. C.; Kosynkin, D. V.; Berlin, J. M.; Sinitskii, A.; Sun, Z.; Slesarev, A.; Alemany, L. B.; Lu, W.; Tour, J. M. Improved Synthesis of Graphene Oxide. *ACS Nano* **2010**, *4*, 4806−4814.

(30) Stöber, W.; Fink, A.; Bohn, E. Controlled Growth of Monodisperse Silica Spheres in the Micron Size Range. *J. Colloid Interface Sci.* **1968**, *26*, 62−69.

(31) Zeng, Q.; Cheng, J.; Tang, L.; Liu, X.; Liu, Y.; Li, J.; Jiang, J. Self-Assembled Graphene−Enzyme Hierarchical Nanostructures for Electrochemical Biosensing. *Adv. Funct. Mater.* **2010**, *20*, 3366−3372.

(32) Etienne, M.; Walcarius, A. Analytical Investigation of the Chemical Reactivity and Stability of Aminopropyl-Grafted Silica in Aqueous Medium. *Talanta* **2003**, *59*, 1173−1188.

(33) Matsuura, K.; Saito, T.; Okazaki, T.; Ohshima, S.; Yumura, M.; Iijima, S. Selectivity of Water-Soluble Proteins in Single-Walled Carbon Nanotube Dispersions. *Chem. Phys. Lett.* **2006**, *429*, 497−502.

(34) Llusar, M.; Monros, G.; Roux, C.; Pozzo, J. L.; Sanchez, C. One-Pot Synthesis of Phenyl- and Amine-Functionalized Silica Fibers through the Use of Anthracenic and Phenazinic Organogelators. *J. Mater. Chem.* **2003**, *13*, 2505−2514.

(35) Wu, S.; Duan, N.; Ma, X.; Xia, Y.; Wang, H.; Wang, Z.; Zhang, Q. Multiplexed Fluorescence Resonance Energy Transfer Aptasensor between Upconversion Nanoparticles and Graphene Oxide for the Simultaneous Determination of Mycotoxins. *Anal. Chem.* **2012**, *84*, 6263−6270.

(36) Chang, H.; Wang, G.; Yang, A.; Tao, X.; Liu, X.; Shen, Y.; Zheng, Z. A Transparent, Flexible, Low-Temperature, and Solution-Processable Graphene Composite Electrode. *Adv. Funct. Mater.* **2010**, *20*, 2893−2902.

(37) Chesne, S.; Rondeau, P.; Armenta, S.; Bourdon, E. Effects Of Oxidative Modifications Induced By the Glycation of Bovine Serum Albumin On its Structure and on Cultured Adipose Cells. *Biochimie* **2006**, *88*, 1467−1477.

(38) Ahmed, M. H.; Byrne, J. A.; McLaughlin, J.; Ahmed, W. Study of Human Serum Albumin Adsorption and Conformational Change on DLC and Silicon Doped DLC Using XPS and FTIR Spectroscopy. *J. Biomater. Nanobiotechnol.* **2013**, *4*, 194−203.

(39) Hu, Z.; Li, J.; Li, C.; Zhao, S.; Li, N.; Wang, Y.; Wei, F.; Chen, L.; Huang, Y. Folic Acid-Conjugated Graphene-ZnO Nanohybrid for Targeting Photodynamic Therapy under Visible Light Irradiation. *J. Mater. Chem. B* **2013**, *1*, 5003−5013.

(40) Akhavan, O.; Ghaderi, E. Graphene Nanomesh Promises Extremely Efficient *in Vivo* Photothermal Therapy. *Small* **2013**, *9*, 3593−3601.

(41) Song, X.; Gong, H.; Liu, T.; Cheng, L.; Wang, C.; Sun, X.; Liang, C.; Liu, Z. J-Aggregates of Organic Dye Molecules Complexed with Iron Oxide Nanoparticles for Imaging-Guided Photothermal Therapy Under 915-nm Light. *Small* **2014**, *10*, 4362−4370.

(42) Tian, Q.; Hu, J.; Zhu, Y.; Zou, R.; Chen, Z.; Yang, S.; Li, R.; Su, Q.; Han, Y.; Liu, X. Sub-10 nm $Fe_3O_4@Cu_{2−X}S$ Core−Shell Nanoparticles for Dual-Modal Imaging and Photothermal Therapy. *J. Am. Chem. Soc.* **2013**, *135*, 8571−8577.

(43) Xie, L.; Tong, W.; Yu, D.; Xu, J.; Li, J.; Gao, C. Bovine Serum Albumin Nanoparticles Modified with Multilayers and Aptamers for pH-Responsive and Targeted Anti-Cancer Drug Delivery. *J. Mater. Chem.* **2012**, *22*, 6053−6060.

(44) Liu, Z.; Sun, X.; Nakayama-Ratchford, N.; Dai, H. Supramolecular Chemistry on Water-Soluble Carbon Nanotubes for Drug Loading and Delivery. *ACS Nano* **2007**, *1*, 50−56.

(45) Li, G.; Song, S.; Guo, L.; Ma, S. Self-Assembly of Thermo- and pH-Responsive Poly(Acrylic Acid)-B-Poly(*N*-Isopropylacrylamide) Micelles for Drug Delivery. *J. Polym. Sci., Part A: Polym. Chem.* **2008**, *46*, 5028−5035.

(46) Mok, H.; Veiseh, O.; Fang, C.; Kievit, F. M.; Wang, F. Y.; Park, J. O.; Zhang, M. pH-Sensitive Sirna Nanovector for Targeted Gene Silencing and Cytotoxic Effect in Cancer Cells. *Mol. Pharmaceutics* **2010**, *7*, 1930−1939.

(47) Padilla-Parra, S.; Matos, P. M.; Kondo, N.; Marin, M.; Santos, N. C.; Melikyan, G. B. Quantitative Imaging of Endosome Acidification and Single Retrovirus Fusion with Distinct Pools of Early Endosomes. *Proc. Natl. Acad. Sci. U. S. A.* **2012**, *109*, 17627−17632.

(48) Chen, H.; Li, S.; Li, B.; Ren, X.; Li, S.; Mahounga, D. M.; Cui, S.; Gu, Y.; Achilefu, S. Folate-Modified Gold Nanoclusters as Near-Infrared Fluorescent Probes for Tumor Imaging and Therapy. *Nanoscale* **2012**, *4*, 6050−6064.